Hindawi
Advances in Civil Engineering
Volume 2020, Article ID 5281725, 16 pages
https://doi.org/10.1155/2020/5281725

Research Article

Experimental Study on Cumulative Damage Behavior of Steel-Reinforced Concrete Columns

Lianjie Jiang[1,2] **and Guoliang Bai**[1]

[1]*School of Civil Engineering, Xi'an University of Architecture & Technology, Xi'an 710055, Shaanxi, China*
[2]*Department of Architectural Engineering, Suqian College, Suqian 223800, Jiangsu, China*

Correspondence should be addressed to Lianjie Jiang; jianglianjie1983@126.com

Received 14 November 2019; Accepted 23 April 2020; Published 30 May 2020

Academic Editor: Rosario Montuori

The cumulative damage behavior of SRC columns under far-field long-period ground motions was simulated and studied by quasi-static tests with the same displacement for 10 times. Quasi-static tests of 8 SRC columns were conducted under the horizontal cyclic loading with the same displacement for 10 times or 3 times, and then the effects of steel ratio, stirrup ratio, axial compression ratio, and number of cyclic loading on the cumulative damage of SRC columns under the far-field long-period ground motions were studied. The results showed that the number of cyclic loading had little effect on the peak load of the specimens, but had a significant effect on the deformation capacity, stiffness degradation, and energy dissipation capacity. Compared with the specimens after 3 cycles, the displacement ductility coefficient of specimens after 10 cycles was reduced by about 20%–26%, the ultimate hysteresis energy dissipation was reduced by 35%–48%, while the stiffness degradation rate was accelerated. After the peak load, the cumulative damage caused by multiple cyclic loading with the same displacement was more significant, which aggravated the reduction of bearing capacity and stiffness degradation. The smaller the steel ratio and stirrup ratio, the larger the axial compression ratio, and the greater the reduction of the bearing capacity and stiffness of specimens. However, accumulated damage caused by multiple cyclic loading with the same displacement had a slight impact on the energy dissipation capacity. Increasing the steel ratio and stirrup ratio can effectively improve the deformation capacity and energy dissipation capacity of the specimens and reduce the bearing capacity and stiffness degradation caused by cumulative damage.

1. Introduction

As a special kind of ground motion, the far-field long-period ground motion has the characteristics of long duration and rich low-frequency components; and in the latter vibration stage, obvious cyclic pulses which are similar to harmonic vibration can be observed [1–3]. The 2011 east Japan earthquake damage and E-Defense shaking table test results show that the high-rise structure with long natural vibration period has the following characteristics under the far-field long-period ground motions: large displacement response, multiple cycles, and long duration with large displacement; and the cyclic number in which the interlayer displacement angle exceeds the elastic-plastic displacement angle limit can reach more than 10 times, and the plastic deformation of multiple reciprocating cycles leads to serious cumulative damage of the high-rise structure [4–9].

Steel-reinforced concrete (SRC) columns are important load-bearing members in high-rise structures. Many experimental researches on seismic performance of SRC columns have been carried out at home and abroad. The low-cycle reversed loading tests of traditional SRC columns were carried out through changing the parameters of axial compression ratio, stirrup ratio, steel distribution form, steel ratio, and shear span ratio; the failure form, hysteresis curve, skeleton curve, bearing capacity, ductility, and energy dissipation capacity of SRC columns were studied [10–14]. The results show that SRC columns have better seismic performance than RC columns. Due to the wide application of high-strength and high-performance concrete, the low-cycle

reversed loading tests of steel reinforcement high-strength and high-performance concrete columns (SRHSHPC) were also performed [15–17], and the failure process and seismic characteristics of SRHSHPC were illustrated. In order to improve the mechanical properties of ordinary SRC columns, scholars proposed novel SRC columns with new-type cross sections, for example, (1) cross-shaped steel, whose flanges were in contact with concrete cover and (2) rotated cross-shaped steel, whose webs coincide with diagonal line of column sections [18, 19]. The results show that, when the steel ratio of the cross-section differs little, the deformation capacity and energy dissipation capacity of the new type of SRC columns is significantly greater than that of the ordinary SRC columns, and the new type of SRC columns still has good bearing capacity and deformation performance under the action of high axial force. However, most of the researches on seismic performance of SRC columns are based on the quasi-static tests of the horizontal cyclic loading for 3 times after yielding, and the effect of far-field long-period ground motions is rarely considered, resulting in the incomplete illustration of cumulative damage and the overestimate of deformation ability in multiple cyclic loading with same displacement [20]. According to the displacement response of high-rise structures under the far-field long-period ground motions, the effect of far-field long-period ground motions was simulated by increasing the number of horizontal cyclic loadings in the quasi-static test, and the cumulative damage performance of RC beams [20], RC columns [21–24], and CFST composite columns [25, 26] was studied under the long-period ground motion. The results show that the number of cyclic loading has little influence on the performance of the components before the peak load and multiple cyclic loading with the larger displacement aggravates the cumulative damage of the components after the peak load; with the increase of the number of cyclic loading, the degradation rate of the strength and stiffness of the components increases, and the deformation capacity decreases significantly. Compared with the standard three times of cyclic loading, the cyclic degradation caused by multiple cyclic loading has a negative impact on the seismic performance of components. At present, research on the cumulative damage performance of SRC columns under long-period far-field ground motion is still rare. To this end, the quasi-static test method of the horizontal cyclic loading for 10 times was adopted to simulate the far-field long-period ground motions, and the quasi-static tests of 8 SRC columns were conducted under the cyclic loading with the same displacement for 10 times or 3 times in this paper, and the influence of steel ratio, stirrup ratio, axial compression ratio, and the number of cyclic loading on the cumulative damage performance of SRC columns was studied comparatively. This study provides an experimental basis for the seismic design of SRC columns.

2. Experimental Process

2.1. Specimen Design. Eight SRC columns with the same geometric dimension were designed in this experiment. The section size of SRC columns was 180 mm × 250 mm, the height was 1200 mm, reinforcing steel bars of 4C16 were arranged longitudinally, the reinforcement ratio was 1.79%; the section size of RC base beam was 400 mm × 700 mm, the length was 1350 mm, and the shear span ratio of specimens was designed as 4.4.

The main change parameters of the specimens included steel ratio, stirrup ratio, axial compression ratio, and number of cyclic loading. Q235 hot rolled I-beams of I12.6, I14, and I16 were used as section steel, with corresponding steel ratios of 4.0%, 4.8%, and 5.8%, respectively; C8@120, C8@100, and C8@80 were used as stirrups (C8@50 was used as column head stirrup), with corresponding stirrup ratios of 1.0%, 1.2%, and 1.5% respectively; the design axial compression ratio was 0.3 and 0.4; the number of cyclic loading was 10 times and 3 times when the displacement angle of column top was not less than 1.0%. Table 1 shows the design parameters of specimens, and Figure 1 shows the specific size and reinforcement.

The concrete design strength grade of the specimens was C40, and the commercial concrete was used. When pouring concrete of the specimens, six 150 mm × 150 mm × 150 mm cubic concrete blocks were made and cured under the same conditions with the specimens. The average cubic compressive strength of concrete blocks was measured to be 49.1 MPa. The properties of steel materials were tested by uniaxial tensile test, and the determined strength indexes are shown in Table 2.

2.2. Loading Devices and Loading System. The "Cantilever column type" quasi-static loading method was adopted. Figure 2 shows the test loading device. Steel beam and anchor screw were used to fix RC base beam on the ground to avoid the horizontal sliding during the loading process. The design axial compression ratio was used to determine the vertical load which was applied to the top of the columns by 1000 kN hydraulic jack and remained constant in the test. The horizontal load was applied by the MTS hydraulic actuator, and the distance between the loading center and the bottom section of the column was 1100 mm. A roller was arranged between the hydraulic jack and the loading steel frame beam to ensure that the hydraulic jack moved with the horizontal displacement of the column top; a one-way rotating hinge was placed between the column top and the hydraulic jack to ensure that the column top can rotate freely in the loading direction.

Displacement control was adopted in the horizontal loading process: the horizontal displacement was step-by-step loaded at displacement angle $\theta = 0.09\%$, 0.18%, 0.23%, 0.3%, 0.36%, 0.45%, 0.6%, and 0.9%, and the displacement of each stage was cycled once; the horizontal displacement was step-by-step loaded at displacement angles $\theta = 1.0\%$, 1.5%, 2.0%, 2.5%, 3.0%, 3.5%, and 4.0%, and the displacement of each stage was cycled multiple times, including 10 cycles for specimens SRC1~SRC6 and 3 cycles for specimens SRC1-2, SRC4-2. When the applied load fell below 85% of the peak load, the test was terminated.

2.3. Measurement Content. In this test, the vertical load, horizontal load, horizontal displacement and strain of section steel flange, web, longitudinal reinforcement, and

Table 1: Design parameters of specimens.

Specimen	Section steel specification	Steel ratio (%)	Stirrup	Stirrup ratio (%)	Design axial compression ratio	Number of cyclic loading
SRC1	I12.6	4.0	C8@100	1.2	0.3	10
SRC2	I14	4.8	C8@100	1.2	0.3	10
SRC3	I16	5.8	C8@100	1.2	0.3	10
SRC4	I14	4.8	C8@120	1.0	0.3	10
SRC5	I14	4.8	C8@80	1.5	0.3	10
SRC6	I14	4.8	C8@100	1.2	0.4	10
SRC1-2	I12.6	4.0	C8@100	1.2	0.3	3
SRC4-2	I14	4.8	C8@120	1.0	0.3	3

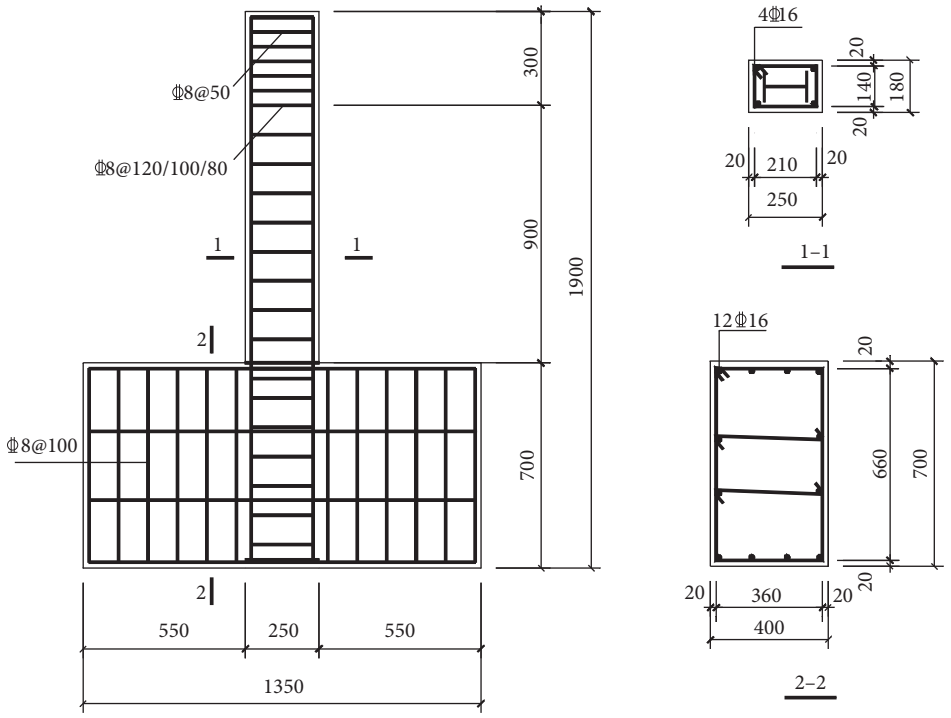

Figure 1: Specimen size and section reinforcement.

Table 2: Steel strength index.

Steel type	Yield strength (MPa)	Ultimate strength (MPa)
I12.6 flange	320.8	448.3
I12.6 web	338.9	452.2
I14 flange	387.5	523.3
I14 web	380.2	484.4
I16 flange	385.8	514.2
I16 web	366.7	480.7
C16	524.7	659.1
C8	453.8	614.7

stirrup of the specimens were measured. The crack development and distribution of the specimens were observed under cyclic loading. The vertical load, horizontal load, and horizontal displacement of the column top were collected in real time by sensors. The horizontal displacement of the RC base beam was monitored by a displacement meter arranged on the side of the base beam. The tensile strain and compressive strain of the section steel flange, web, longitudinal reinforcement, and stirrup were measured by resistance strain gauge pasted in the steel and collected by the DH3816 static strain test system.

3. Results and Discussion

3.1. Damage Process and Failure Mode. Since the failure process and failure mode of each specimen are similar, SRC4 is specifically analyzed in the limited space. The failure process of SRC4 is divided into three stages: precracking, damage development, and failure. The test phenomena in each stage are as follows.

Precracking stage: before the cracking load of the specimen. When the displacement angle is not more than 0.23%, there is no visible change in the specimen; when the displacement angle is 0.3%, the first horizontal crack about

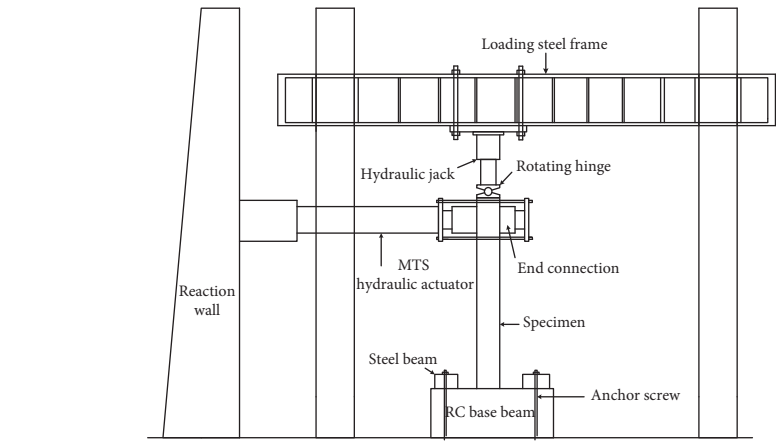

(a)

(b)

Figure 2: Test loading device. (a) Schematic diagram of test loading device. (b) Field test loading device.

50 mm long appears on the tensile side of the column bottom, reaching the cracking load.

Damage development stage: from cracking load to peak load. With the increase of the displacement angle, the existing cracks of the specimen develop continuously. Several horizontal cracks are generated simultaneously and mainly concentrated in the bottom of the column within the range of 1 times the height of the column section. When the displacement angle is 1.0%, horizontal cracks of the specimen are basically complete, and the inclined cracks appear, extend, and intersect; the longitudinal bars and stirrups begin to yield. When the displacement angle is 1.5%, the vertical cracks appear at the corners of the specimen, the concrete cover begins to peel and peel off in a small amount, the development of existing horizontal cracks and inclined cracks is slow, and the damage of the specimen is not serious, as shown in Figure 3(a). When the displacement angle is 2.0%, the load of specimen reaches the peak load. With the increase of the number of cyclic loading, the horizontal cracks at the bottom of the column gradually develop and widen and the crack width reaches 0.8 mm, 1.0 mm, and 1.3 mm after the 1st, 6^{th}, and 10th cycles respectively; the vertical cracks also extend upward and widen, the crack width reaches 0.5 mm, 1.0 mm, and 2.0 mm after the 1st, 4^{th}, and 10th cycles, respectively, accompanied by the fall of the concrete cover, and the damage degree of the specimen gradually aggravates, as shown in Figure 3(b).

Failure stage: from the peak load to failure. When the displacement angle is 2.5%, the number of cyclic loadings has more influence on the damage process of the specimen. Horizontal cracks at the bottom of the column continue to widen with the increase of the number of cyclic loading, and most of the concrete cover between the two horizontal cracks at the bottom of the column fall off after the 3rd cycle. Vertical cracks also extend upward and widen obviously in multiple cycles, the maximum width after the 1st, 3^{rd}, and 6th cycles reaches 2.0 mm, 3.0 mm, and 5.5 mm, respectively, and the damage and falling off area of the concrete cover increases greatly. Figures 3(c)–3(e) show the failure modes of the specimen after the 1st, 6^{th}, and 10th cycles, respectively. During the 1st cycle with displacement angle of 3.0%, the concrete cover within the range of 1 time the column section height at the bottom of the column is crushed and falls off in large area, the longitudinal reinforcement and stirrup are exposed outwards, the longitudinal reinforcement is bent and bulged, and the section steel is partially bent. The damage of the specimen develops rapidly, and the bearing capacity decreases sharply, leading to the serious failure. The final failure mode of the specimen is shown in Figure 3(f).

Figure 3: Failure mode of specimens. (a) SRC4 (1.5%). (b) SRC4 (2.0%). (c) SRC4 (2.5%-1st). (d) SRC4 (2.5%-6th). (e) SRC4 (2.5%-10th). (f) SRC4 (failure). (g) SRC1. (h) SRC2. (i) SRC3. (j) SRC1-2. (k) SRC4-2.

The failure modes of other specimens are basically the same. The failure mainly occurs in the range of 250 mm–300 mm at the bottom of the column. During the failure, the concrete cover is severely crushed and peeled off, the longitudinal reinforcement and stirrup are exposed and buckled, and section steel is partially buckled, which belongs to the bending failure. Figures 3(g)–3(k) show the failure modes of other specimens.

It is found that multiple cyclic loading has certain influence on the cumulative damage and failure process of the specimens. Compared with the specimens after 3 cycles, the specimens after 10 cycles have an increasing crack width at the same displacement angle in the cyclic loading, and the corresponding displacement angle decreases with the same failure characteristics. For example, when the displacement angle is 2.0%, the maximum width of the horizontal crack of SRC4-2 is 0.5 mm, while that of SRC4 is 1.3 mm; when the concrete cover is seriously peeled off and the specimen is damaged, the corresponding displacement angles of SRC4-2 are about 3.0% and 3.5% respectively, while the corresponding displacement angles of SRC4 are about 2.5% and 3.0%, respectively.

3.2. Hysteresis Curves. The hysteresis curves of horizontal load P and displacement angle θ of all specimens are shown in Figure 4. It can be concluded that

(1) The hysteresis curves of the specimens are full and fusiform, without obvious pinch phenomenon, indicating that the specimens have good energy dissipation capacity. Before the peak load, with the increase of the number of cyclic loading, the bearing capacity of the specimens decreases slightly, and the stiffness degradation is not obvious. After the peak load, with the increase of displacement amplitude and the number of cyclic loading, the damage accumulation of the specimens increases continuously and the bearing capacity and stiffness degradation are more significant.

(2) Through the comparison of specimens SRC1, SRC2, and SRC3, the steel ratio has obvious influence on the hysteresis performance of the specimens. With the increase of the steel ratio, the peak load of the specimens is greatly improved, the hysteresis curve is fuller, and the energy dissipation capacity is stronger; through the comparison of specimens SRC2, SRC4, and SRC5, after the peak load, the bearing capacity and stiffness of the specimen with larger stirrup ratio degrade slowly and the ultimate displacement angle increases greatly. This is because section steel and stirrup can effectively restrain the core concrete and improve the cooperative working ability of the core concrete and section steel, so as to improve the hysteresis performance of the specimens. At the same time, it is found that when the displacement angle is more than 2.5%, the bearing capacity and stiffness of SRC4 degenerate suddenly and significantly. The analysis shows that the stirrup spacing of SRC4 is larger, which weakens the effective constraints on the section steel frame and the core area concrete; and the concrete cover is severely crushed and peels off at the latter stage of loading, resulting in the significant degradation of bearing capacity and stiffness.

(3) As shown in hysteresis curves of specimens SRC2 and SRC6, when the axial pressure ratio is small, the hysteresis loop of the specimen is relatively full. When the load of the specimen reaches the peak load, the hysteresis curve is relatively stable, the ultimate displacement angle is large, and the energy dissipation capacity is strong. With the increase of the axial pressure ratio, the hysteresis curve of the specimen becomes thin, the bearing capacity and stiffness degrade sharply, the ultimate displacement angle and the number of cyclic loading reduce, and the deformation capacity and energy dissipation capacity decrease.

(4) The number of cyclic loading has a significant effect on the hysteresis properties of the specimens. The hysteresis loops of specimens SRC1-2 and SRC4-2 after 3 cycles are full. After the peak load, the hysteresis curves are stable, the reduction of bearing capacity and stiffness degeneration is slow, the ultimate displacement angle is large, and the energy dissipation capacity is strong. On the contrary, hysteresis curves of specimens SRC1 and SRC4 after 10 cycles decrease in fullness. After the peak load, bearing capacity and stiffness degrade rapidly and the ultimate displacement angle and energy dissipation capacity decrease. This phenomenon is mainly caused by the accumulated damage of the specimen under the action of multiple cyclic loading.

3.3. Deformation Capacity. According to the skeleton curve of the specimens, the yield displacement Δ_y, yield displacement angle θ_y, peak displacement Δ_{max}, peak displacement angle θ_{max}, ultimate displacement Δ_u, and ultimate displacement angle θ_u of all specimens are determined, and the displacement ductility coefficients u of specimens are calculated by $u = \Delta_u/\Delta_y$ [27]. The results are listed in Table 3. The values in the table are the average values of displacement, displacement angle, and displacement ductility coefficient under positive and reverse loading. The yield displacement Δ_y is determined by the equal energy method [28], and the limit displacement Δ_u is the displacement corresponding to the horizontal load falling to 85% of the peak load. In this paper, the ultimate displacement angle θ_u [29] and the displacement ductility coefficient u are used to describe the deformation capacity of the specimens. From Table 3, it is concluded that

(1) The deformation capacity of the specimens decreases with the increase in the number of cyclic loading. For specimens SRC1-2 and SRC4-2 after 3 cycles, θ_u is, respectively, 2.95% and 3.53%, which is much more than 2.0%; u is, respectively, 2.93 and 3.02, which are close to 3.0. This indicates that specimens SRC1-2 and SRC4-2 after 3 cycles have good deformation ability. With the increase of the number of cyclic loading, the damage of the specimens is accumulated. θ_u and u of SRC1 after 10 cycles decrease by 12.5% and 26.6% than those of SRC1-2; θ_u and u of SRC4 decrease by 43.3% and 20.5% than those of SRC4-2, respectively. Therefore, the cumulative damage greatly reduces the deformation ability of the specimen.

(2) The larger the steel ratio and stirrup ratio, the better the deformation ability of the specimen. For specimens SRC1, SRC2, and SRC3, with the increase of steel ratio, θ_u and u increase. Comparing SRC1 with the minimum steel ratio, θ_u and u of SRC3 with the maximum steel ratio increase by 17.4% and 18.6%, respectively. Compared with SRC2, SRC4, and SRC5, with the increase of stirrup ratio, θ_u and u increase gradually. Compared with SRC4, θ_u and u of SRC5 increase by 11.5% and 11.3%, respectively. This is because the effective restraint effect of section steel and stirrup on the concrete in the core area lead to three-dimensional compression state for the

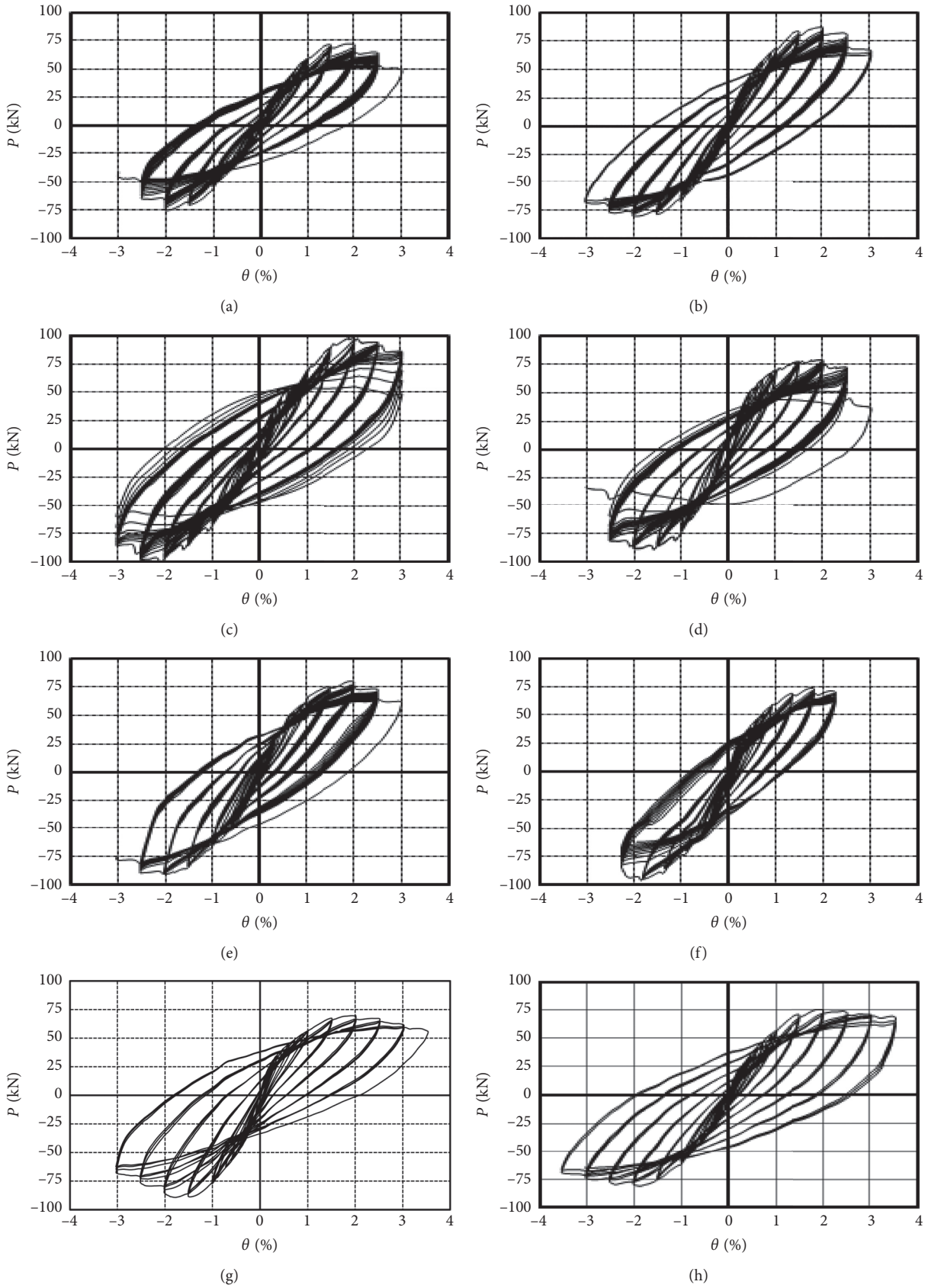

Figure 4: Hysteresis curves of horizontal load and displacement angle ($P-\theta$) of specimens. (a) SRC1. (b) SRC2. (c) SRC3. (d) SRC4. (e) SRC5. (f) SRC6. (g) SRC1-2. (h) SRC4-2.

Table 3: Bearing capacity and deformation capacity of specimens.

Specimen	P_y (kN)	Δ_y (mm)	θ_y (%)	P_{max} (kN)	Δ_{max} (mm)	θ_{max} (%)	Δ_u (mm)	θ_u (%)	u
SRC1	62.2	13.17	1.20	73.2	22.20	2.02	28.34	2.58	2.15
SRC2	71.2	12.66	1.15	83.3	22.20	2.02	31.88	2.90	2.52
SRC3	79.9	13.05	1.28	96.8	22.20	2.02	33.30	3.03	2.55
SRC4	72.1	11.88	1.08	82.8	22.20	2.02	28.55	2.60	2.40
SRC5	71.9	11.94	1.09	85.0	22.20	2.02	31.86	2.90	2.67
SRC6	70.0	12.31	1.12	84.0	20.10	1.83	25.00	2.27	2.03
SRC1-2	65.8	11.06	1.01	78.0	19.50	1.77	32.46	2.95	2.93
SRC4-2	65.7	12.86	1.17	76.9	22.20	2.02	38.85	3.53	3.02

concrete in the core area of the specimen, and thus the deformation ability of the specimen improves.

(3) The deformation capacity of the specimen decreases with the increase of axial compression ratio. By comparison, θ_u and u of SRC6 with large axial compression ratio are 21.7% and 19.4% lower than those of SRC2 with small axial compression ratio, respectively. Because in the latter stage of loading, the P-Δ effect of the specimen with the large axial compression increases, and the additional bending moment accelerates the failure process, reduces the ultimate deformation, and weakens the deformation ability.

3.4. Bearing Capacity

3.4.1. Test Value of Bearing Capacity. Table 3 shows measured values of yield load P_y and peak load P_{max} of all specimens. The results show the following:

(1) The load of most specimens reaches the peak load when the displacement angle is about 2.0%, the peak load is about 1.15–1.21 times of the yield load, and the average value is 1.18 times.

(2) The number of cyclic loading has little effect on the peak load. Compared with those of SRC1-2 and SRC4-2 after 3 cycles, the peak load of SRC1-2 and SRC4-2 after 10 cycles decreases by 6.1% and increases by 7.6%, respectively, and changes slightly overall. Combined with the damage development, it is analyzed that the damage development of the specimens is relatively slow and the damage accumulation is not serious before the peak load, so the impact on the peak load is small.

(3) The peak load of SRC3 with the largest steel ratio is significantly greater than that of other specimens, which is about 1.32 times of SRC1 with the smallest steel ratio. This indicates that increasing the steel ratio can effectively improve the bearing capacity of the specimens.

(4) The peak load of SRC2, SRC4, and SRC5 with different stirrup ratio has little difference. The average value is 83.7 kN, and the maximum difference is 1.5%. This suggests that the influence of stirrup ratio on the peak load is small, and there is a limited effect of increasing stirrup ratio on improving the bearing capacity of the specimens.

(5) Although increasing the axial compression ratio can enhance the restraint effect on the specimen, the increase of the axial compression ratio does not significantly increase the peak load of the specimen.

3.4.2. Effect of Cumulative Damage on Bearing Capacity Decline. With the increase of the number of cyclic loading, the damage of the specimens accumulates and the bearing capacity of the specimens decreases. The ratio P_i/P_1, where P_i is the maximum horizontal load at the ith cycle of the same displacement and P_1 is the maximum horizontal load at the 1st cycle, is used to investigate the reduction of bearing capacity of specimens caused by cumulative damage. The larger the ratio, the smaller the reduction of bearing capacity. Table 4 shows the calculation results of P_3/P_1 and P_{10}/P_1 of the specimens under different displacement angle cycles. From Table 4, following conclusions are made:

(1) In the same displacement angle cycle, $P_{10}/P_1 < P_3/P_1$, indicating that the bearing capacity of the specimens, decreases with the increase of the number of cycle loading.

(2) The reduction of bearing capacity is related to the amplitude of displacement angle. When the displacement angle is 1.0% and 1.5%, the specimens cannot yield or reach the peak load, P_{10}/P_1 is about 0.940–0.997 and slightly less than P_3/P_1, and the bearing capacity drops slightly. It shows that the cumulative damage of specimens caused by the multiple cyclic loading with the small displacement has little influence on the reduction of bearing capacity. When the displacement angle is 2.0%, the bearing capacity of the specimens reaches the peak load and the reduction range of bearing capacity begins to increase. The bearing capacity of the specimen SRC1 decreases by 12.3% in the 10th cycle, and the bearing capacity of the remaining specimens decreases by no more than 8.0%, indicating that the cumulative damage has a certain impact on the reduction of the bearing capacity of the specimen. When the displacement angle is 2.5% and 3.0%, the bearing capacity of the specimens decreases less than 7.0% in the 3rd cycle. However, with the increase of the number of cycle loading, the damage of specimens develops rapidly. In the 10th cycle, the bearing capacity of most specimens decreases more than

Table 4: P_3/P_1 and P_{10}/P_1 of specimens with different displacement angles.

Specimen	Displacement angle (%)	P_3/P_1	P_{10}/P_1
SRC1	1.0	0.984	0.984
	1.5	0.973	0.940
	2.0	0.940	0.877
	2.5	0.941	0.786
SRC2	1.0	0.964	0.950
	1.5	0.967	0.945
	2.0	0.965	0.924
	2.5	0.962	0.885
	3.0	0.944	—
SRC3	1.0	0.967	0.964
	1.5	0.971	0.951
	2.0	0.981	0.973
	2.5	0.984	0.936
	3.0	0.973	0.703
SRC4	1.0	0.989	0.976
	1.5	0.985	0.963
	2.0	0.983	0.937
	2.5	0.974	0.739
SRC5	1.0	0.989	0.997
	1.5	0.990	0.991
	2.0	0.977	0.956
	2.5	0.968	0.907
	3.0	—	—
SRC6	1.0	0.993	0.993
	1.5	0.986	0.984
	2.0	0.973	0.952
	2.5	0.949	0.847
	3.0	—	—
SRC1-2	1.0	0.972	—
	1.5	0.965	—
	2.0	0.950	—
	2.5	0.942	—
	3.0	0.935	—
SRC4-2	1.0	0.980	—
	1.5	0.964	—
	2.0	0.954	—
	2.5	0.951	—
	3.0	0.962	—

Note. Specimen SRC3 is cycled for 8 times at the displacement angle of 3%, and in the table $0.703 = P_8/P_1$.

10.0%, and the maximum decrease is 26.1%. The above analysis shows that serious cumulative damage is caused by multiple cycles of larger displacement, which greatly reduces the bearing capacity of specimens. The bearing capacity index measured by 3 standard cycle tests is obviously high.

(3) For specimens SRC1, SRC2, and SRC3, after the peak load, the larger the steel ratio, the larger the P_3/P_1 and P_{10}/P_1 and the smaller the reduction of bearing capacity of the specimens. For example, in the 10th cycle with displacement angle of 2.0% and 2.5%, the bearing capacity of SRC1 with the minimum steel ratio decreases by 12.3% and 21.4%, respectively, while that of SRC3 with the maximum steel ratio only decreases by 2.7% and 6.4%, respectively. Therefore, increasing the steel ratio can reduce the reduction of the bearing capacity caused by the cumulative damage.

(4) For specimens SRC2, SRC4, and SRC5, after the peak load, with the increase of the stirrup ratio, P_3/P_1 and P_{10}/P_1 of the specimens increase and the reduction of bearing capacity decreases. For example, in the 10th cycle with displacement angles of 2.0% and 2.5%, the bearing capacity of SRC4 with minimum stirrup ratio decreases by 6.3% and 26.1%, while that of SRC5 with maximum stirrup ratio decreases by 4.4% and 9.3%, respectively. Therefore, increasing the stirrup ratio is beneficial to reduce the adverse effect of cumulative damage on the bearing capacity of specimens.

(5) For specimens SRC2 and SRC6, before the peak load, the bearing capacity of SRC6 with a large axial pressure ratio decreases slightly with the increase of the number of cyclic loadings, since the large axial pressure enhances the end restraint of the specimen; after the peak load, the bearing capacity of SRC6 decreases rapidly and the bearing capacity decreases 15.3% at the displacement angle of 2.5% in the 10th cycle, while the bearing capacity of SRC2 with the smaller axial compression ratio is reduced by 11.5%. It can be seen that, in the later stage of loading, the larger the axial compression ratio, the larger the reduction of the bearing capacity of the specimen. This is because the larger axial pressure results in the greater additional bending moment, which aggravates the degradation of the bearing capacity of the specimen.

3.5. Secant Stiffness

3.5.1. Average Secant Stiffness. Due to the elastic-plastic property and cumulative damage of the specimens, the stiffness decreases with the increase of displacement amplitude and the number of cyclic loadings. Secant stiffness K is the ratio of the sum of the absolute values of the maximum positive and negative horizontal load and the sum of the absolute values of the maximum horizontal displacement at each cycle. Figure 5 shows the relation curves between the average secant stiffness K_m and the displacement angle θ of the specimens. K_m refers to the secant stiffness which is obtained by dividing the sum of secant stiffness of multiple displacement loading cycle by the number of loading cycles [26]. The meaning of "average hysteresis energy dissipation" below is similar to K_m. It can be seen that, with the increase of displacement angle, the average secant stiffness of the specimens decreases linearly, and the steeper the $K_m - \theta$ curves, the more significant the stiffness degradation of the specimens.

As shown in Figure 5(a), the stiffness degradation of SRC4-2 after 3 cycles is relatively gentle and that of SRC4 after 10 cycles is significantly fast; when the displacement angle is 3.0%, K_m of SRC4 is about 50% lower than that of SRC4-2. It indicates that the cumulative damage caused by multiple cycles of displacement accelerates the rate of stiffness degradation. As shown in Figure 5(b), during the

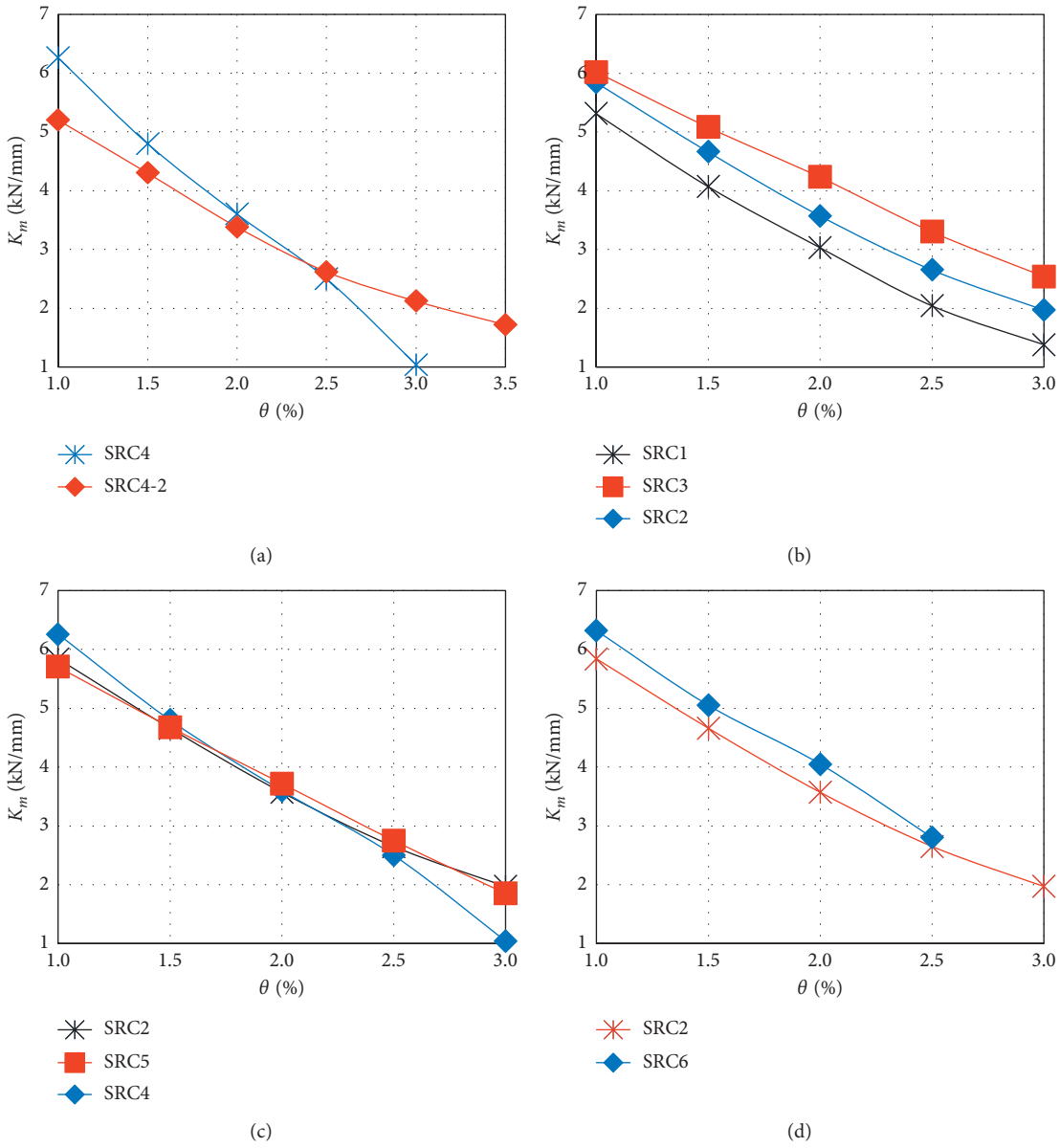

FIGURE 5: Relation curves of average secant stiffness-displacement angle ($K_m - \theta$) of specimens. Effect of (a) cyclic loading number on K_m, (b) steel ratio on K_m, (c) stirrup ratio on K_m, and (d) axial compression ratio on K_m.

same displacement angle, with the increase of steel ratio, the stiffness of the specimen increases gradually and the stiffness degradation rate tends to slow down. As shown in Figure 5(c), the stiffness degradation of SRC4 with the minimum stirrup ratio is faster. With the increase of stirrup ratio, $K_m - \theta$ curve of the specimen gradually becomes flat and the stiffness degradation rate slows down. As shown in Figure 5(d), the greater the axial compression ratio, the greater the stiffness of the specimen. Before the peak load, the stiffness degradation rate of all specimens is basically the same; after the peak load, $K_m - \theta$ curve of the specimen SRC6 with the greater axial compression ratio is steeper and the stiffness degradation is faster. This is also related to the more significant P-Δ effect of large axial compression specimen.

3.5.2. Effect of Cumulative Damage on Secant Stiffness Degradation. As mentioned above, with the increase of the number of cyclic loading, the stiffness of the specimens also decreases. The relation curves between secant stiffness K and cycle number N of the specimens are shown in Figure 6, where $N = 1$–10 is the cycle number of 1.0% displacement angle, $N = 11$–20 is the cycle number of 1.5% displacement angle, $N = 21$–30 is the cycle number of 2.0% displacement

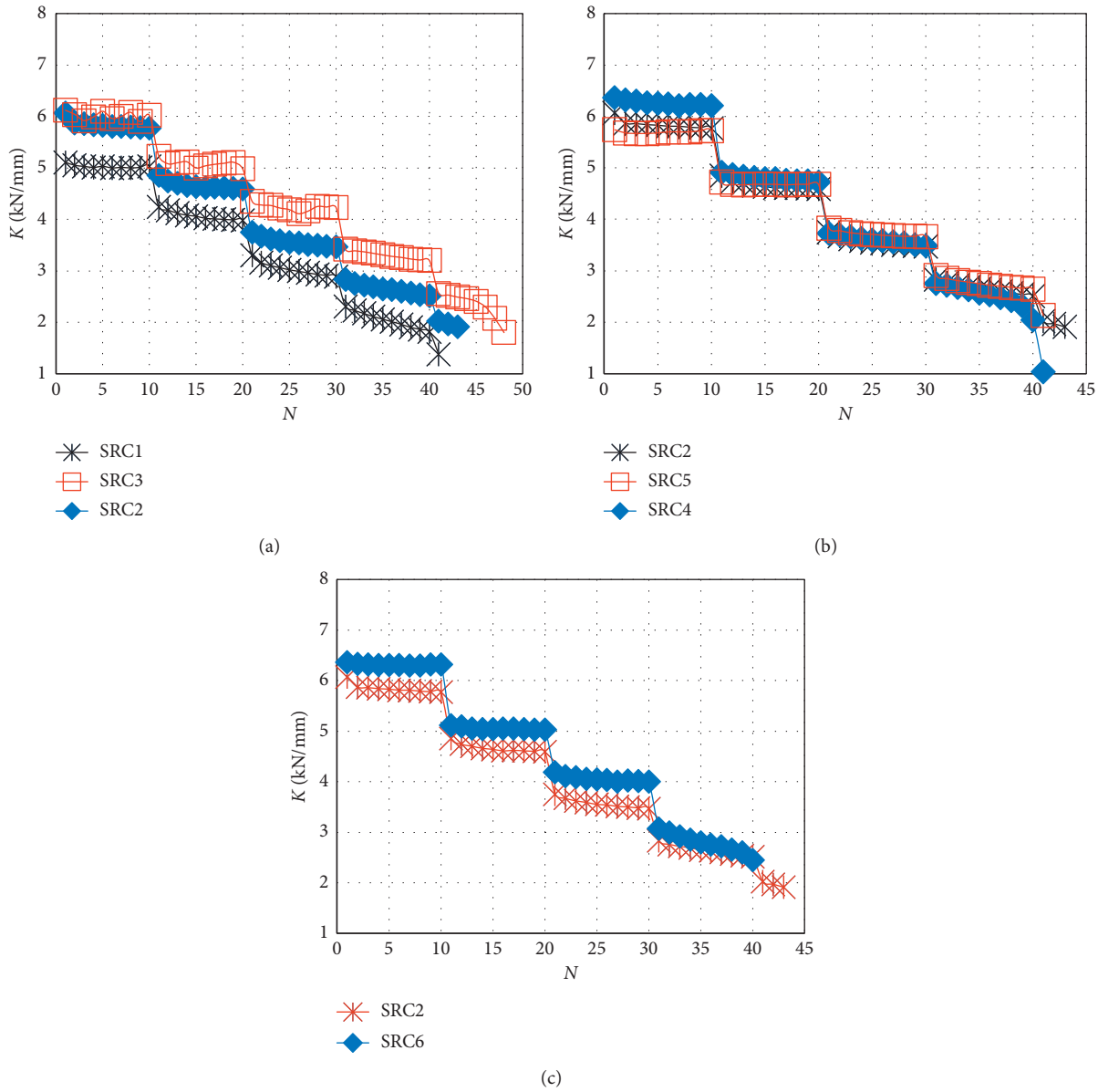

FIGURE 6: Secant stiffness-cycle loading number K-N curves of specimens. Effect of (a) steel ratio on K, (b) stirrup ratio on K, and (c) axial compression ratio on K.

angle, $N = 31–40$ is the cycle number of 2.5% displacement angle, and $N = 41–50$ is the cycle number of 3.0% displacement angle. With reference to P_i/P_1, the ratio K_i/K_1 is used to reflect the stiffness degradation of specimens caused by cumulative damage, in which K_i is the secant stiffness in the ith cycle of the same displacement and K_1 is the secant stiffness in the 1st cycle.

According to Figure 6(a), when the displacement angle is 1.0% and 1.5%, with the increase of the number of cyclic loading, the stiffness of the specimens decreases slight, K_{10}/K_1 is more than 0.95 in the 10th cycle; when the displacement angle is 2.0% and 2.5%, the stiffness reduction range of the specimens increases with the increase of the number of cycles, K_3 decreases within 5.0% in the 3rd cycle; the reduction range of K_{10} increases to 6.0%–20.0% in the 10th cycle, and the lower the steel ratio, the greater the reduction range of stiffness. When the displacement angle is 3.0%, the K–N curve of specimen SRC3 develops unsteadily and the stiffness decreases sharply in the 5th cycle. The above analysis shows that the accumulated damage caused by multiple cycles of large displacement is more serious after the peak load, which aggravates the stiffness degradation of the specimens. Increasing the steel ratio can reduce the adverse effect of the accumulated damage on the stiffness degradation to a certain extent.

According to the analysis of Figures 6(b)–6(c), when the displacement angle is 1.0%, 1.5%, and 2.0%, with the increase of the number of cyclic loading, the stiffness reduction of the specimens with different stirrup ratios and axial compression ratios is not significant, indicating that the cumulative

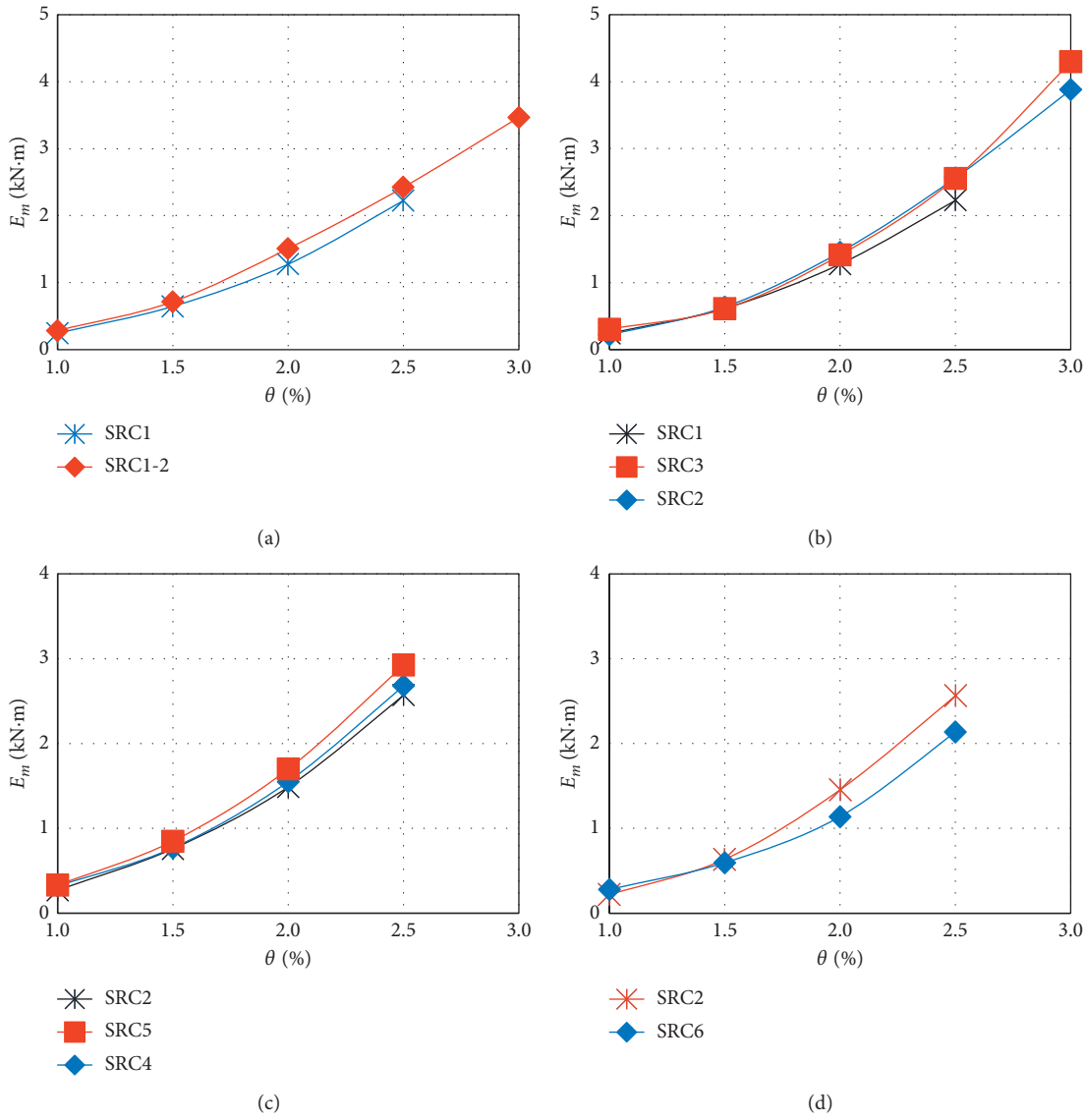

FIGURE 7: Relation curves of average hysteresis energy-displacement angle ($E_m - \theta$) of specimens. Effect of (a) cyclic loading number on E_m, (b) steel ratio on E_m, (c) stirrup ratio on E_m, and (d) axial compression ratio on E_m.

damage is not serious, and the impact on the stiffness degradation of the specimens is small; when the displacement angle is 2.5%, the smaller the stirrup ratio, the greater the axial compression ratio, and the greater the stiffness reduction. The maximum reduction can be up to 20.2%, and the stiffness degradation rate obviously accelerates.

3.6. Energy Dissipation Capacity

3.6.1. Average Hysteresis Energy. The hysteresis energy dissipation capacity can comprehensively reflect the influence of displacement amplitude and cyclic loading number on the damage accumulation of components. Figure 7 shows the relation curves between the average hysteresis energy E_m and the displacement angle θ of the specimens, where the hysteresis energy of the specimens in each cycle is the area surrounded by the corresponding P-θ hysteresis curve. From Figure 7, it is concluded that

(1) With the increase of the displacement angle, the damage degree, the average hysteresis energy, and the energy dissipation capacity of the specimens increase.

(2) When the displacement angle is 1.0% and 1.5%, the average hysteresis energy of specimens is almost the same. When the displacement angle exceeds 1.5%, the number of cyclic loading, steel ratio, stirrup ratio, and axial compression ratio all have great influence on the energy dissipation capacity of the specimens. Specific analysis shows that the average hysteresis energy of SRC1 after 10 cycles is about 8%–15% lower than that of SRC1-2 after 3 cycles, which indicates that the cumulative damage caused by

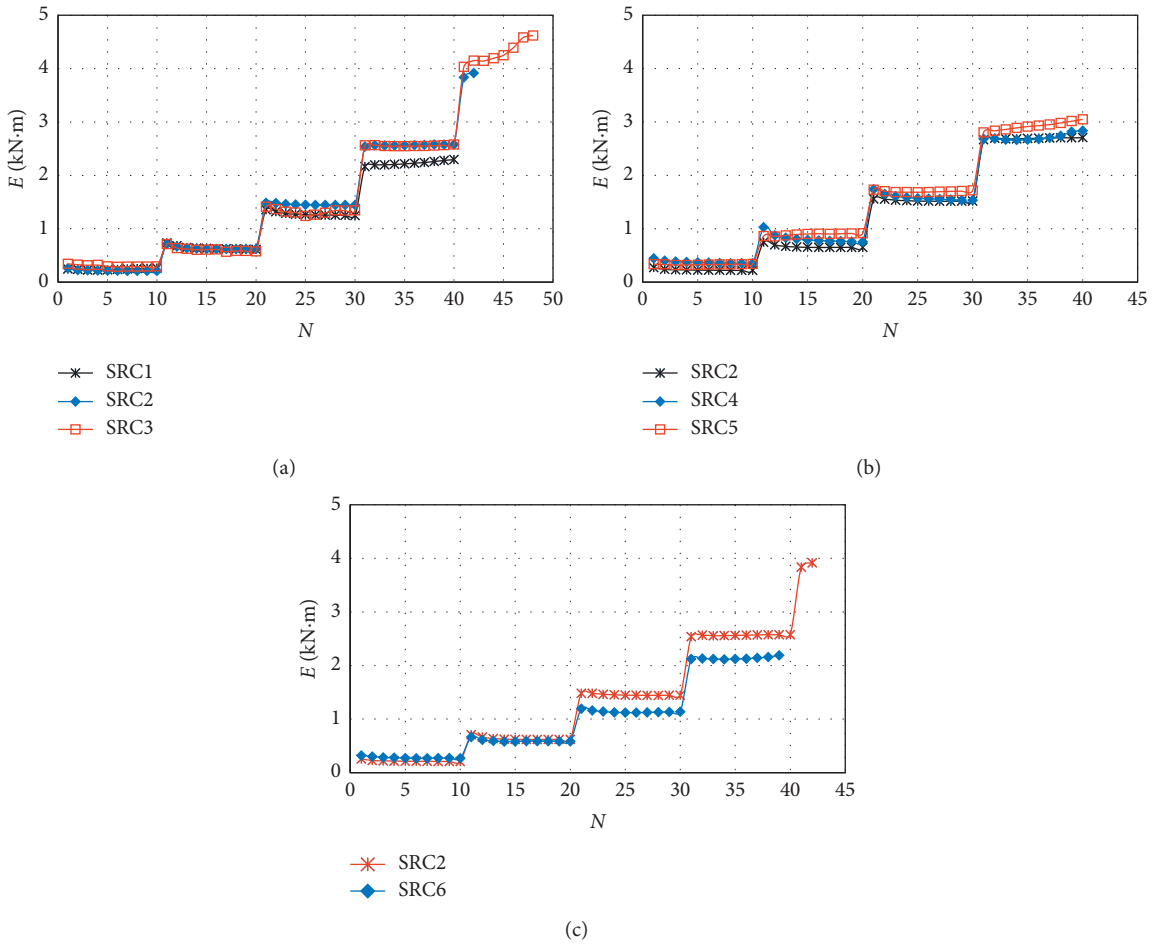

FIGURE 8: Relation curves between hysteresis energy-cycle loading number E-N of specimens. Effect of (a) steel ratio on E, (b) stirrup ratio on E, and (c) axial compression ratio on E.

multiple cycles with large displacement reduces the energy dissipation capacity of the specimens. The larger the steel ratio and stirrup ratio, the greater the average hysteresis energy and the stronger the energy dissipation capacity. Thus, increasing the steel ratio and stirrup ratio can effectively improve the energy dissipation capacity of the specimens. The average hysteresis energy of SRC6 with large axial compression ratio is significantly lower than that of SRC2 with small axial compression ratio. It indicates that the larger the axial compression ratio, the worse the energy dissipation capacity of the specimen.

3.6.2. Effect of Cumulative Damage on Hysteresis Energy Dissipation. Figure 8 shows the relation curves between the hysteresis energy E and the number of cycle loading N, and the corresponding relation between N and the displacement angle θ is the same as that described in Section 3.5.2. As shown in Figure 8, when the displacement angle is 1.0%, 1.5%, and 2.0%, with the increase of the number of cyclic loading, the hysteresis energy of the specimens is basically the same or slightly decreased and the decrease range is not more than 10%. It suggests that the cumulative damage caused by multiple cycles of displacement is slight and has little impact on the energy dissipation of the specimens. When the displacement angle is 2.5% and 3.0%, the hysteresis energy of the specimens remains the same or slightly increased with the increase of the number of cyclic loading, and the maximum increase range is 8.0%. Hence, the cumulative damage still has little influence on the energy dissipation capacity of the specimens. When the displacement angle is 3.5%, with the increase of the number of cycles, the damage degree of SRC3 increases gradually, the hysteresis energy increases rapidly, and the energy dissipation capacity increases continuously.

In general, the cumulative damage has little effect on the energy dissipation capacity of the specimens. When the specimen approaches failure, due to the increase of cumulative damage degree, the energy dissipation capacity still increases with the increase of the number of cycle loading to some extent although the horizontal load of the specimen decreases significantly.

3.6.3. Ultimate Hysteresis Energy and Ultimate Equivalent Viscous Damping Coefficient. When the specimen reaches the failure state, the corresponding hysteresis energy and

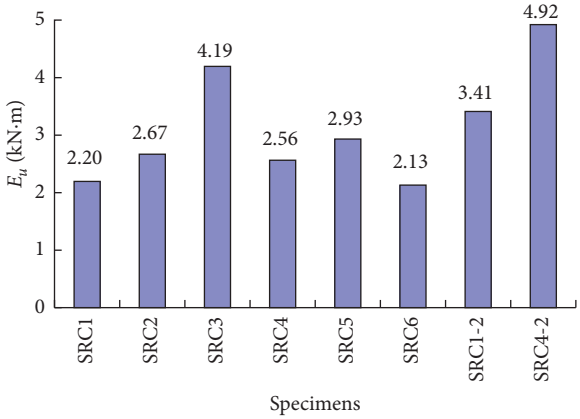

Figure 9: Ultimate hysteresis energy of specimens.

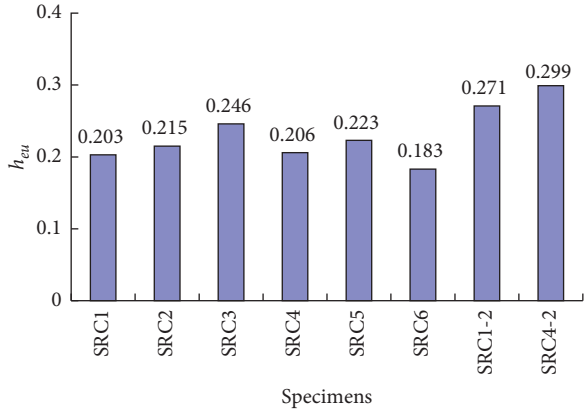

Figure 10: Ultimate equivalent viscous damping coefficient of specimens.

equivalent viscous damping coefficient are defined as the ultimate hysteresis energy E_u and the ultimate equivalent viscous damping coefficient h_{eu}, respectively. E_u and h_{eu} can reflect the ultimate energy dissipation capacity of the specimen [28]. The larger E_u and h_{eu}, the stronger the ultimate energy dissipation capacity of the specimen. The horizontal load falling to 85% of the peak load is taken as the failure criterion of the specimen. The displacement amplitude and hysteresis curve corresponding to the failure of the specimens are determined, and E_u and h_{eu} of each specimen are calculated. The calculation results are shown in Figures 9 and 10. It can be concluded that

(1) When the failure state is reached, the ultimate equivalent viscous damping coefficient h_{eu} of the specimens is 0.183–0.299, mostly above 0.2, which is greater than the ultimate equivalent viscous damping coefficient 0.1–0.2 of RC columns with bending failure [30]. It indicates that the SRC columns have better energy dissipation capacity than the RC columns.

(2) With the increase of steel ratio and stirrup ratio, E_u and h_{eu} of the specimens increase gradually. E_u and h_{eu} of SRC3 with the maximum steel ratio are 1.9 times and 1.21 times than those of SRC1with the minimum steel ratio, respectively; and E_u and h_{eu} of SRC5 with the maximum stirrup ratio are 1.14 times and 1.08 times than those of SRC4 with the minimum stirrup ratio, respectively. It can be concluded that increasing the steel ratio and stirrup ratio can improve the ultimate energy dissipation capacity of the specimens, and increasing the steel ratio is more effective.

(3) E_u and h_{eu} of SRC2 with small axial compression ratio are larger than those of SRC6 with a large axial compression ratio. Therefore, the ultimate energy dissipation capacity of the specimens decreases with the increase of the axial compression ratio.

(4) The number of cyclic loading has the greatest influence on the ultimate energy dissipation capacity of the specimens. E_u and h_{eu} of the specimens after 10 cycles are significantly lower than those of the specimens after 3 cycles. The former is only 0.52–0.65 times and 0.69–0.75 times of the latter, respectively. The cumulative damage greatly reduces the ultimate energy dissipation capacity of the specimens.

4. Conclusion

The cumulative damage behavior of SRC columns under far-field long-period ground motions was simulated and studied by quasi-static tests with the same displacement for 10 times. Through the quasi-static tests of 8 SRC columns under the cyclic loading with the same displacement for 10 or 3 times, the test phenomena and results are comprehensively analyzed. The conclusions are drawn as follows:

(1) Bending failure is the main failure mode of the specimens. During the failure, the concrete cover is severely crushed and peeled off, the longitudinal reinforcement and stirrup are exposed and buckled, and the section steel is partially buckled. Compared with the specimens after 3 cycles, specimens after 10 cycles have a larger crack width at the same displacement angle cycle, smaller displacement angle at the same failure characteristics, and more significant failure degree.

(2) For the specimens subjected to the cyclic loading of same displacement for 10 times, increasing the steel ratio can improve the peak load of the specimens, and increasing the stirrup ratio has less effect on increasing the peak load of the specimens. With the increase of steel ratio and stirrup ratio, the deformation capacity and energy dissipation capacity of the specimens enhance, and the rate of stiffness degradation slows down. With the increase of the axial compression ratio, the deformation capacity and energy dissipation capacity of the specimens decrease, and the stiffness degradation rate increases at the later stage of loading.

(3) With the increase of the number of cyclic loading, the cumulative damage of 10 cycles before the peak load is slight, which has little impact on the bearing capacity, secant stiffness, and energy dissipation

capacity of the specimens; after the peak load, the cumulative damage caused by multiple cycles of displacement is serious, and the reduction range of bearing capacity and stiffness of the specimens in the 10th cycle is greater than that in the 3rd cycle; and the smaller the steel ratio and stirrup ratio, the larger the axial compression ratio and the larger the reduction range of the specimens. Besides, increasing the steel ratio and stirrup ratio can effectively reduce the reduction range of the bearing capacity and stiffness of the specimens caused by multiple cycles of the same displacement cumulative damage.

(4) The number of cyclic loading has a significant effect on the cumulative damage performance of the specimens. Compared with specimens after 3 cycles, the peak load of the specimens after 10 cycles changes slightly, while the fullness of the hysteresis curve decreases, the deformation capacity and the ultimate energy dissipation capacity decrease, and the stiffness degradation is more significant after the peak load.

Data Availability

The data used to support the findings of this study are included within the article.

Conflicts of Interest

The authors declare that they have no conflicts of interest.

Acknowledgments

This work was supported by the National Natural Science Foundation of China (51878544), the Natural Science Foundation of the Jiangsu Higher Education Institutions of China (18KJD560005), and the Natural Science Basic Research Plan in Shaanxi Province of China (2019JM-597), which are gratefully acknowledged.

References

[1] K. Koket and H. Miyake, "A seismological overview of long-period ground motion," *Journal of Seismology*, vol. 12, no. 2, pp. 133–143, 2008.

[2] L. J. Xu, J. J. Hu, and L. L. Xie, "On characteristics of ground motion parameters for special long period ground motions," *Journal of Earthquake Engineering and Engineering Vibration*, vol. 28, no. 6, pp. 20–27, 2008.

[3] Y. Cheng and G. L. Bai, "Basic characteristic parameters and influencing factors of long-period ground motion records," *Journal of Vibroengineering*, vol. 19, no. 7, pp. 5191–5207, 2017.

[4] I. Takewaki, S. Murakami, K. Fujita, S. Yoshitomi, and M. Tsuji, "The 2011 off the Pacific coast of Tohoku earthquake and response of high-rise buildings under long-period ground motions," *Soil Dynamics and Earthquake Engineering*, vol. 31, no. 11, pp. 1511–1528, 2011.

[5] F. L. Zhou, H. C. Cui, A. Shigetaka et al., "Inspection report of the disaster of the East Japan earthquake by Sino-Japanese joint mission," *Building Structure*, vol. 42, no. 4, pp. 1–20, 2012.

[6] Y.-L. Chung, T. Nagae, T. Hitaka, and M. Nakashima, "Seismic resistance capacity of high-rise buildings subjected to long-period ground motions: E-defense shaking table test," *Journal of Structural Engineering*, vol. 136, no. 6, pp. 637–644, 2010.

[7] X. Ji, G. L. Fenves, K. Kajiwara, and M. Nakashima, "Seismic damage detection of a full-scale shaking table test structure," *Journal of Structural Engineering*, vol. 137, no. 1, pp. 14–21, 2011.

[8] C. F. Liang, B. H. Pan, Z. M. Ma, Z. H. He, and Z. H. Duan, "Utilization of CO2 curing to enhance the properties of recycled aggregate and prepared concrete: a review," *Cement and Concrete Composites*, vol. 105, Article ID 103446, 2020.

[9] S. N. Vandanapu and M. Krishnamurthy, "Seismic performance of lightweight concrete structures," *Advances in Civil Engineering*, vol. 2018, Article ID 2105784, 6 pages, 2018.

[10] S. El-Tawil and G. G. Deierlein, "Strength and ductility of concrete encased composite columns," *Journal of Structural Engineering*, vol. 125, no. 9, pp. 1009–1019, 1999.

[11] J. Sakai and C. Matsui, "Hysteresis characteristic of steel reinforced concrete beam-columns: formulae on skeleton curves of SRC beam-columns encased H-shaped steel," *Journal of Structural and Construction Engineering (Transactions of AIJ)*, vol. 65, no. 534, pp. 183–190, 2000.

[12] C. C. Weng and S. I. Yen, "Comparisons of concrete-encased composite column strength provisions of ACI code and AISC specification," *Engineering Structures*, vol. 24, no. 1, pp. 59–72, 2002.

[13] J. Shi and G. L. Bai, "An experimental study on restoring force characteristics of lattice type steel reinforced concrete frame columns," *Journal of Xi'an Highway University*, vol. 20, no. 4, pp. 94–97, 2000.

[14] Z. X. Guo, Z. W. Zhang, and Y. Liu, "Tentative study on the seismic performance and index for different performance level of SRC columns," *Journal of Xi'an University of Architecture and Technology (Natural Science Edition)*, vol. 41, no. 5, pp. 593–598, 2009.

[15] J. H. Li, X. T. Wang, J. Y. Xue, and H. T. Zhao, "Experimental study on the performance of steel reinforced high-strength concrete columns under low cyclic reversed loading," *China Civil Engineering Journal*, vol. 40, no. 7, pp. 11–18, 2007.

[16] B. Wang, S. S. Zheng, X. F. Guo, F. Yu, and H. R. Zhang, "Seismic damage analysis for SRHSHPC frame columns," *Engineering Mechanics*, vol. 29, no. 2, pp. 61–68, 2012.

[17] W. Q. Zhu, G. Meng, and J. Q. Jia, "Experimental studies on axial load performance of high-strength concrete short columns," *Proceedings of the ICE: Structures and Buildings*, vol. 167, no. 9, pp. 509–519, 2014.

[18] M. Fukuhara and K. Minami, "Seismic performance of new type steel-concrete composite structures considering characteristic both SRC and CFT structures," in *Proceedings of the World Conference on Earthquake Engineering*, Beijing, China, October 2008.

[19] Q. W. Wang, Q. X. Shi, W. S. Jiang, X. H. Zhang, W. Hou, and Y. Tian, "Experimental study on seismic behavior of steel reinforced concrete columns with new-type cross sections," *Journal of Building Structures*, vol. 34, no. 11, pp. 123–129, 2013.

[20] X. Y. Sun, *Experimental Study on the Seismic Performance of Frame Beam with Simulating the Long-Period Seismic Loads*, Beijing University of Technology, Beijing, China, 2013.

[21] K. Kawashima and T. Koyama, "Effect of number of loading cycles on dynamic characteristics of reinforced concrete bridge pier columns," *Structural Engineering/Earthquake Engineering: JSCE*, vol. 5, no. 1, pp. 183–191, 1988.

[22] J. R. Qian and B. R. Feng, "Experimental study on seismic behavior of different seismic grade RC columns," *Journal of Building Structures*, vol. 35, no. 7, pp. 105–114, 2014.

[23] S. Pujol, M. A. Sozen, and J. A. Ramirez, "Displacement history effects on drift capacity of reinforced concrete columns," *ACI Structural Journal*, vol. 103, no. 2, pp. 253–262, 2006.

[24] B. Acun and H. Sucuoğlu, "The effect of displacement history on the performance of concrete columns in flexure," *Advances in Performance-Based Earthquake Engineering*, vol. 13, pp. 373–382, 2010.

[25] X. D. Ji, M. L. Zhang, and P. Liu, "Experimental study of cumulative damage performance of steel tube-reinforced concrete composite columns," *Journal of Building Structures*, vol. 34, no. 12, pp. 35–44, 2013.

[26] J. R. Qian, N. B. Li, X. D. Ji, and W. L. Cao, "Experimental study on cumulative damage performance of composite-sectioned high strength concrete-filled steel tubular columns," *China Civil Engineering Journal*, vol. 47, no. 2, pp. 30–40, 2014.

[27] C. L. Zhou, X. W. Li, D. B. Wang, and S. X. Xia, "Analysis of bearing capacity and seismic performance of circular RC columns strengthened with externally wrapped steel plates," *Advances in Civil Engineering*, vol. 2019, Article ID 2515091, 17 pages, 2019.

[28] J. C. Zhu, J. X. Gong, L. J. Xiong, J. L. Qiu, and X. Li, "Experimental study on the seismic behavior of reinforced concrete bridge piers under varied loading cycles," *Journal of Southeast University (Natural Science Edition)*, vol. 49, no. 4, pp. 652–663, 2019.

[29] R. Fusco, R. Montuori, E. Nastri, and V. Piluso, "Critical analysis of ultimate rotation formula for R.C. columns subjected to cyclic loadings," *Engineering Structures*, vol. 177, pp. 160–174, 2018.

[30] J. Y. Xue, H. Ma, and Y. Liu, "Experimental study on seismic performance of steel reinforced recycled concrete columns under low-cyclic reversed loading," *China Civil Engineering Journal*, vol. 47, no. 1, pp. 36–46, 2014.